Abdom Imaging 21:433–439 (1996)

Abdominal Imaging

Liver MR imaging: comparison of respiratory triggered fast spin echo with T2-weighted spin-echo and inversion recovery

M. T. Keogan,[1] C. E. Spritzer,[1] E. K. Paulson,[1] S. S. Paine,[1] L. Harris,[1] J. L. Dahlke,[2] J. R. MacFall[1]

[1]Department of Radiology, Duke University Medical Center, Durham, NC 27710, USA
[2]GE Medical Systems, Milwaukee, WI, USA

Received: 5 April 1995/Accepted: 2 May 1995

Abstract

Background: The purpose of this study was to compare a fast spin-echo sequence combined with a respiratory triggering device (R. trig. FSE) with conventional T2-weighted spin-echo (CSE) and inversion recovery (STIR) sequences for the detection of focal hepatic lesions.

Methods: We performed a prospective study of 33 consecutive patients with known or suspected hepatic tumors. All patients underwent R. trig. FSE, CSE, and STIR imaging at 1.5 T. Acquisition times were 10.7 min for the CSE sequence and ranged from 12 to 15 min for STIR and from 5 to 7 min for R. trig FSE. For each sequence, liver–spleen contrast-to-noise ratio (CNR) and liver–lesion CNR were determined quantitatively. Image artifact and sharpness were graded by using a four-point scale on each sequence by two independent readers. Both readers also independently identified hepatic lesions (up to a maximum of eight per patient). For patients with focal lesions, the total number of lesions detected (on each sequence) and the minimum size of detected lesions were also determined by each reader.

Results: No significant difference was detected between R. trig. FSE and CSE or STIR in either liver–spleen CNR or liver–lesion CNR. R. trig. FSE images were equivalent to CSE and superior to STIR in sharpness ($p < 0.01$) and presence of artifact ($p < 0.01$). R. trig. FSE detected a higher number of lesions (reader 1: n = 92, reader 2: n = 86) than CSE (reader 1: n = 70, reader 2: n = 69) and a significantly higher number than STIR (reader 1: n = 71, reader 2: n = 76). Lesion structure was significantly better defined with R. trig. FSE than with STIR ($p < 0.01$) and CSE ($p < 0.05$).

Conclusions: Compared with CSE and STIR, R. trig. FSE produces hepatic images of comparable resolution and detects an increased number of focal hepatic lesions in a shorter period of time.

Key words: Magnetic resonance—Fast spin echo—Liver.

Correspondence to: M. T. Keogan

For high field strength hepatic magnetic resonance (MR) imaging, conventional T2-weighted spin-echo sequences (CSE) are more sensitive than T1-weighted spin-echo sequences for lesion detection [1] and, hence, are a mainstay of diagnosis. A disadvantage of T2-weighted sequences, however, is the long acquisition time, which increases susceptability to respiratory and motion artifacts [2]. These artifacts may be partially improved by respiratory compensation techniques [3].

Fast spin-echo sequences (FSE), which also produce heavily T2-weighted sequences, have been evaluated in the upper abdomen and pelvis with variable results [4–8]. Despite the shorter acquisition time for FSE versus CSE sequences, artifacts related to respiratory motion remain a significant problem affecting image quality and lesion detection. At this time, respiratory compensation techniques compatible with FSE sequences are not commercially available. Breath-held FSE sequences may reduce respiratory artifact and are under evaluation by several groups [9, 10]. As breath-holding may be difficult for some patients, we attempted to couple an alternative technique, respiratory triggering, with FSE imaging. Respiratory triggering has been described as an effective technique for the reduction of respiratory artifact and is best suited to a sequence with a long repetition time (TR) [9].

The purpose of this study is to compare an FSE sequence that employs respiratory triggering to standard

CSE and inversion recovery (STIR) sequences for overall hepatic image quality and hepatic lesion detection. STIR sequences have been shown to be effective at 1.5 T [12, 13] and recently have been shown to be equivalent in sensitivity to computed tomography (CT) with arterial portography [12]. For this reason, STIR sequences have been routinely used at our institution as a adjunct to CSE and were therefore included in this comparative study.

Materials and Methods

Subjects

Thirty-three consecutive patients (20 men and 13 women, aged 18–58 years) with known or suspected hepatic pathology underwent hepatic MR imaging during a 6-month period (July to December 1993). Thirty patients had biopsy-proven malignancy and had one or more focal hepatic abnormalities on CT (n = 13 colon carcinoma, 8 breast carcinoma, 2 rectal carcinoma, 2 melanoma, 2 hepatoma, 1 sarcoma, 1 Hodgkin's disease, and 1 gallbladder carcinoma); three patients had no known malignancies (diagnoses included one case of pancreatitis, one of heaptic adenoma, and one of weight loss with a questionable CT hepatic abnormality). Eighteen of these patients underwent CT-guided biopsy and had malignancy confirmed in at least one lesion; 15 of these had multiple lesions on imaging. Four patients with multiple liver lesions had evidence of widespread extrahepatic malignancy and did not undergo biopsy. In the remaining three patients, each with a solitary lesion, two cysts and one hemangioma were described based on T2 calculations. These lesions were stable for at least 1 year based on repeat CT examinations.

Imaging Protocol

MR imaging was performed on a 1.5-T system (Signa 5X; GE Medical Systems Milwaukee, WI). R. trig. FSE was compared with two inevitability slower sequences: (1) conventional T2-weighted spin echo to provide a T2-weighted sequence for comparison and (2) STIR, which at our institution has been validated as a sensitive sequence for detection of focal hepatic abnormalities [14]. For all sequences, spatial presaturation pulses were applied above and below the liver to reduce blood flow artifacts; section thickness to spacing was 7 mm to 3 mm, and identical section locations were chosen. The field of view varied from 28 to 34 cm. Conventional T2-weighted spin-echo (TR/TE = 2500/40,80 ms) sequences were performed as follows: 256 × 128 matrix, two excitations, first-moment flow compensation, and respiratory compensation (reordering of phase-encoding steps). Images obtained with a TE of 80 were used for comparison with the other two sequences. The liver was typically imaged in one acquisition (20–22 slices per acquisition). Acquisition time was 10.7 min.

STIR sequence parameters were as follows: TR/TE/TI = 2000–3000/40/148–155 (TI was adjusted to the null point for each patient), 256 × 128 matrix, and one excitation. Flow compensation, respiratory compensation, and spatial presaturation were used as for the CSE sequence. The bandwidth was reduced to ±8 kHz and to ±16 kHz for the CSE and FSE sequences. Two acquisitions were typically obtained (8–10 slices per acquisition). Acquisition time ranged from 12 to 15 min.

For R. trig. FSE imaging, the parameters were adjusted to optimize the sequence rather than to replicate CSE sequence. The TR varied depending on the patient's respiratory rate and pattern, which activated the respiratory triggering device, and was typically between 3000 and 6000 ms. The effective TE was 102 ms. The matrix was 256 × 256, two signals were averaged, echo train length was 8, and echo spacing was 16 ms. Flow compensation in the frequency direction was applied. Fat saturation was used to counteract the additional signal obtained from fat with FSE sequences [15].

The respiratory triggering device is an in-house modification of the existing (commercially available) cardiac triggering device (Fig. 1A). The respiratory signal is derived from an air bellows wrapped around the thorax and upper abdomen, which produces a signal corresponding to the respiratory phase. This signal is processed via a filter to remove baseline drifts and to give a trigger signal only on expiration (Fig. 1B). The respiratory trigger pulse is routed into the cardiac trigger input of the scanner. The trigger point on the respiratory waveform chosen by the circuit is illustrated in Figure 1C. The trigger point (adjustable for each patient) is set to occur midway between peak inspiration and end expiration. Acquisition then continues for a fixed time period and is not terminated by a premature inspiration. For this reason, in cases where preliminary inspection of the respiratory waveform reveals marked respiratory variation, the trigger point may be set to occur earlier in expiration so that the acquisition may be completed before the onset of a new inspiration. In this study, respiratory variation did not prevent the use of respiratory triggering in any patient. Figure 1C shows the placement of the radio frequency (RF) and gradient pulses for the FSE sequence. Because the acquisition begins at a fixed point in expiration, the respiratory rate determines the TR. Two to three acquisitions were obtained, and the number of slices per acquisition varied between four and eight according to the patient's respiratory rate. Acquisition time ranged from 5 to 7 min.

In a previous study, FSE options including respiratory triggering, gradient moment nulling (frequency and/or slice direction), cardiac gating, randomized phase encoding, breath-holding, and varying echo train lengths were assessed in volunteers and patients not included in this study [16]. Use of the respiratory triggering device and gradient moment nulling (frequency direction) were the most important determinants of image quality. This evaluation resulted in the FSE sequence parameters employed here, and it determined that FSE without respiratory triggering would not be evaluated in this study.

Quantitative Image Analysis

All examinations were assessed quantitatively. Separate regions of interest (ROI) of constant size (400 mm^2) were placed in the right lobe of the liver and the spleen to avoid lesions, vessels, or artifacts when present. A large rectangular ROI, which was used to calculate noise, was placed ventral to the patient. This measurement includes systematic noise and noise caused by artifact from respiration and vessel pulsatility, which is propagated along the phase-encoding direction [13, 18]. For each sequence, ROI values were recorded on as many slices of each sequence as possible, and mean values of liver and spleen signal and noise were calculated for each sequence. When hepatic lesions were present, the largest lesions were identified (maximum of four lesions per patient), and ROIs were adjusted to the size of the lesion to include all areas of tumor heterogeneity. The same lesions were measured for each of the three sequences. For ROI measurement, lesions were evaluated if larger than 200 nm^2; the maximum ROI obtained was 600 mm^2. Each lesion measured was considered separately for liver–lesion contrast-to-noise ratio (CNR) evaluation. From the ROI values, the following parameters were calculated: (1) liver–spleen CNR = (signal liver − signal spleen)/SD noise, (2) liver–lesion CNR = (signal liver − signal lesion)/SD noise, and (3) lesion signal-to-noise ratio = signal lesion/SD noise. Statistical analyses of the data were performed by repeated measures analysis of variance (ANOVA).

Qualitative Image Analysis

The three sequences for each patient were separated and then reviewed independently by two readers experienced in hepatic MR and who did

not participate in the ROI measurements. The readers were blinded to the sequence parameters used. On occasion, certain characteristic features (e.g., chemical shift artifact on STIR images) would have allowed sequence identification. For each sequence, the following criteria were assessed: (1) image sharpness (including sharpness of organ boundaries and vessels) was graded on a four-point scale: poor (significantly blurred organ margins and/or poor vessel definition), fair (moderate blurring), good (minimal blurring), or very good (very sharp boundaries), and (2) presence of artifact (including respiratory, peristaltic, and vascular), graded as severely degrading (80–100% of image), moderately degrading (30–60% of image), minimally degrading (10–30%), and not significant (<10% of image). A pretest evaluation of cases not included in this study was performed by each reader to improve consistancy in evaluation of these criteria. The data on image sharpness was compressed from the original four categories into two categories (good/very good and fair/poor) to maximize overall differences for analysis. Similarly, data on artifact was compressed for analysis into two categories of minimal/not significantly degrading and moderately/severely degrading. McNemar's test was used to test the differences in the correlated proportions.

Each reader identified any hepatic lesions present by segment on each sequence. A concensus reading was not performed. Each reader's data were analyzed separately to provide two independent data sets. A maximum of eight lesions were counted in patients with multiple focal hepatic abnormalities. Pathological confirmation of each individual lesion identified was not obtained as a minority of patients underwent surgical exploration. For this reason, lesions were only considered real for each reader if seen on at least two of three sequences by that reader. This determination was made at the time of statistical analysis, and as a result lesions were described in 25 of 33 patients (by both readers).

The lesion margins were described as blurred or sharp. The composition of each lesion was described as homogeneous, heterogeneous (containing areas of mixed signal intensity), or heterogeneous with visible structure or septations. Statistical analysis of the data was performed by a repeated measures ANOVA.

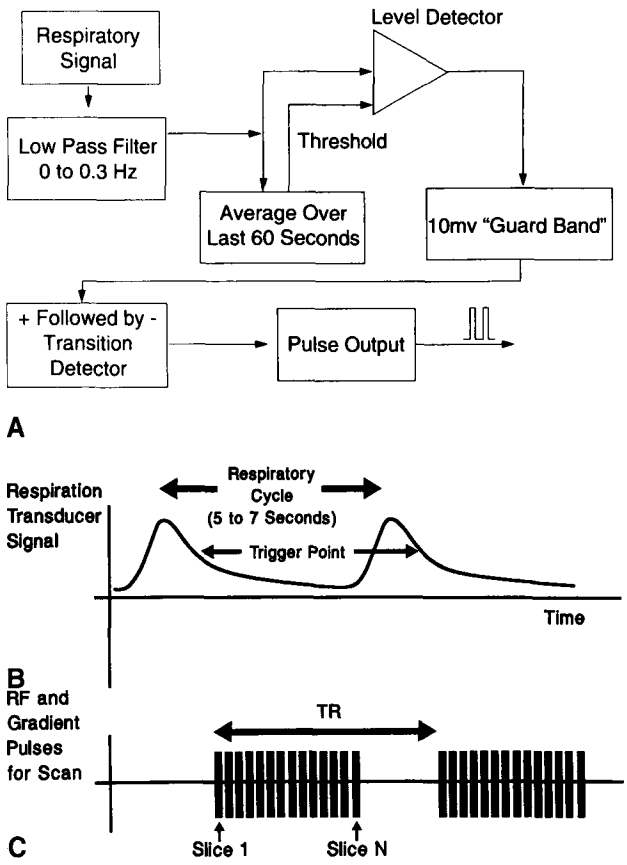

Fig. 1. A Block diagram of the respiratory signal circuit. The respiratory signal is an analog voltage waveform that is derived from a pneumatic bellows around the subject. The signal is filtered to derive the average (nominally zero) voltage that serves to select a trigger point. Triggers that correspond to inspiration are eliminated by a detector that only creates output when the signal makes a transition from positive voltage to negative voltage. Spurious triggers due to slow passage through zero are eliminated by a 10-mV "guard band" circuit that prevents retrigger until the signal has passed above or below this level. **B,C** Respiratory trigger scheme: diagram shows the relationship of the respiratory and pulse sequence waveforms for triggering of the fast spin-echo (FSE) pulse sequence. **B** shows an idealized respiratory waveform signal from the respiratory transducer and circuit. The circuit triggers the start of the pulse sequence when the waveform crosses the half-amplitude point after peak inspiration. In **C**, the black bars show the FSE pulses for each imaged slice. Each bar corresponds to the 90° and 180° pulses for a given slice at a single phase-encoding value. The repetition time is determined by the time between breaths. The number of slices that can be imaged is restricted to those that fit in the minimal motion time between the trigger pulse and the next inspiration. This results in some deliberate inefficiency to avoid data acquisition during inspiration.

Results

Quantitative

No significant difference was detected between R. trig. FSE and either CSE or STIR in terms of liver–spleen CNR (Table 1). Analysis of liver–lesion CNR demonstrated a significant difference between the mean values for the three sequences, $p = 0.02$ (Table 1). To determine the source of this significant difference in liver–lesion CNR, two sequences were then compared consecutively. This analysis revealed no significant difference between R. trig. FSE and CSE ($p = 0.66$) or between R. trig. FSE and STIR ($p = 0.21$); however, STIR was significantly greater than CSE ($p < 0.01$).

Qualitative

Analysis of artifacts for both readers showed no significant difference between R. trig. FSE and CSE ($p > 0.5$), whereas R. trig. FSE and CSE images were significantly better than STIR ($p < 0.01$) (Fig. 2A). Analysis of images with good/very good image sharpness similarly demonstrated no significant difference between R. trig. FSE and CSE ($p > 0.5$), but both sequences were better than STIR ($p < 0.01$) (Figs. 2B, 3). The left lobe of the liver was best seen on the R. trig FSE sequence (Fig. 4), although this finding was not subject to statistical analysis.

Both readers detected lesions on at least two sequences in 25 patients. The total number of lesions de-

Table 1. Quantitative measurements (mean ± SD) of respiratory triggered (R. trig.) FSE compared with CSE and STIR

	R. trig. FSE	CSE	STIR	ANOVA p value*
Liver–spleen CNR	10.96 ± 5.20	9.47 ± 5.76	10.58 ± 6.10	0.34
Liver–lesion CNR	10.84 ± 4.97	9.33 ± 4.31	11.43 ± 5.12	0.02

FSE = fast spin echo, CSE = conventional spin echo, STIR = short tau inversion recovery, CNR = contrast-to-noise ratio
* p value for differences between the means of the three sequences (ANOVA)

tected per sequence for reader 1 was: R. trig. FSE: 92, CSE; 70, STIR; 71, for reader 2: R. trig. FSE: 86, CSE: 69, STIR: 76. By comparing the mean number of lesions detected (total number of lesions detected by one sequence and verified on at least one other sequence per total number, i.e., 25, of patients in whom lesions were seen), both readers found a higher mean number of lesions with R. trig. FSE than with CSE (significant for reader 1: $p = 0.005$), and both found a significantly higher number with R. trig. FSE than with STIR (reader 1: $p = 0.009$; reader 2: $p = 0.005$).

The margins of the hepatic lesions were seen as sharpest with R. trig FSE by both readers, and this reached significance for reader 2 when comparing R. trig FSE with STIR ($p < 0.05$) (Fig. 5). Well-defined internal architecture and septations were seen significantly more often by both readers with R. trig. FSE than with CSE or STIR ($p < 0.05$) (Fig. 5). Detected lesions ranged from 0.6 to 12 cm.

No significant difference was seen between the three sequences in terms of ability to detect small lesions. The minimum size of detected lesions was R. trig. FSE: 0.5 cm, CSE: 0.6 cm, and STIR: 0.6 cm for reader 1 and R. trig. FSE: 0.6 cm, CSE: 0.6 cm, and STIR: 0.6 cm for reader 2.

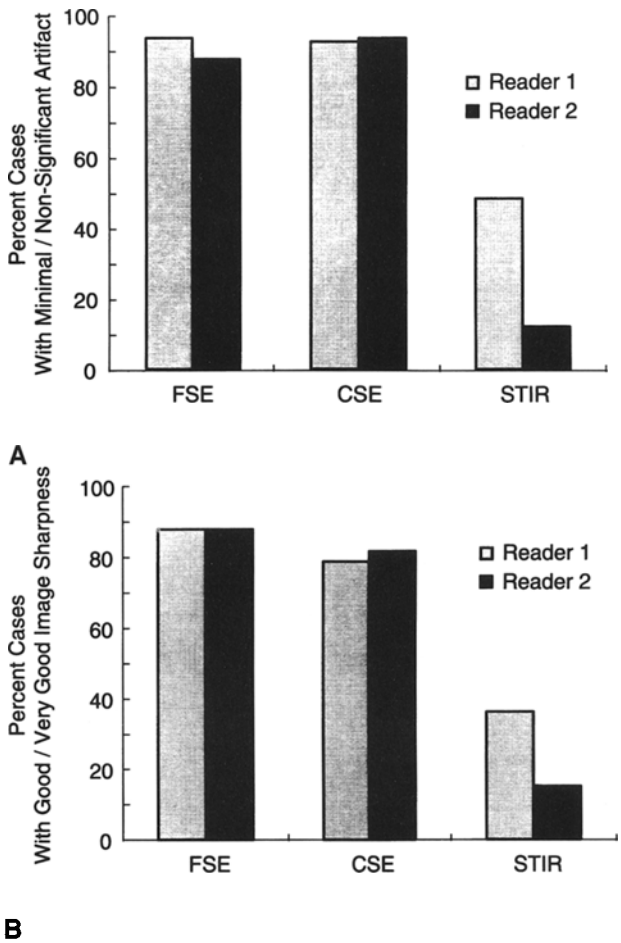

Fig. 2. Qualitative assessment of R. trig. FSE, CSE, and STIR. **A** Percent of cases with minimal or nonsignificant artifact. **B** Percent of cases with good/very good image sharpness.

Discussion

The role of FSE sequences in abdominal MR imaging has been investigated in several papers [4–6, 19]. This sequence was developed from the RARE sequence [20] and provides strongly T2-weighted spin-echo contrast in a much shorter period of time than CSE with improved signal-to-noise and contrast-to-noise ratios [21, 22]. The imaging time for the FSE sequence, even with the addition of respiratory triggering, is much less than the CSE sequence. We elected to use some of this time saving to boost image resolution by increasing the R. trig. FSE matrix size to 256 × 256 versus 256 × 128 for CSE, resulting in an R. trig FSE sequence acquisition in 5–7 min versus CSE acquisition in 10.7 min. Although there was no statistically significant difference between R. trig. FSE and CSE in terms of artifact or image sharpness, there was a trend toward better image quality with the R. trig. FSE images ($p > 0.5$). The improvement in the FSE images compared with CSE may reflect the matrix difference as the 256 × 256 matrix used for R. trig. FSE produces a voxel size one-half that of the 256 × 128 matrix used for the conventional spin-echo sequences.

Artifact due to respiratory motion may be reduced by several techniques. Breath-holding has been used effectively with gradient recalled sequences [23], and definitive studies on the role of breath-holding with FSE are awaited. Respiratory compensation techniques, based on reordering of phase-encoding data and used with standard spin-echo sequences, are effective for mo-

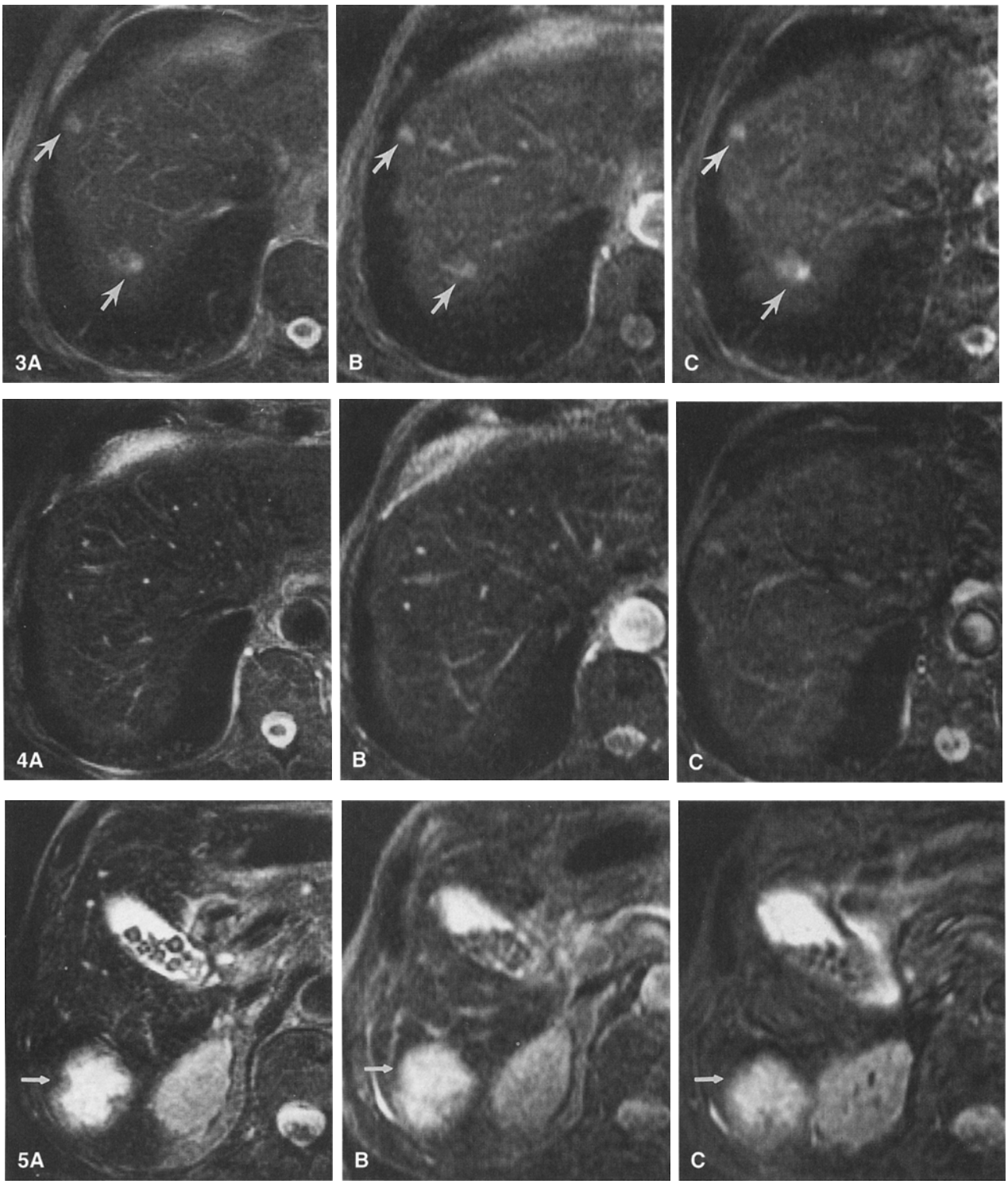

Fig. 3. MR images of the dome of the liver in a patient with metastasis (*arrows*) from breast cancer. **A** R. trig. FSE. **B** CSE. **C** STIR. Note severe image degradation due to motion artifact in the STIR image. Time of image acquisition for the R. trig. FSE sequence was 6 min 20 s versus 10.7 min for the CSE sequence and 15 min for the STIR sequence.

Fig. 4. MR images of the liver in a patient with colon cancer metastases. **A** R. trig. FSE. **B** CSE. **C** STIR. Note the improved visualization of the left lobe on the R. trig. FSE sequence versus the CSE or the STIR sequences.

Fig. 5. MR images of the liver in a patient with colon cancer metastasis. **A** R. trig. FSE. **B** CSE. **C** STIR. The margins and internal structure of the metastatic lesion (*arrow*) are best seen on the R. trig. FSE sequence.

tion reduction. Respiratory compensated FSE, however, is not currently commercially available.

Alternative approaches to reduce respiratory artifact are respiratory triggering and gating techniques [11, 24, 25]. The respiratory gating technique acquires data during end expiration only. Artifacts are significantly reduced, but imaging time is increased by a factor of 2 or 3; thus, this technique is useful only for sequences with a short TR. Respiratory triggering is an alternative technique where the acquisition begins at a fixed point on the respiratory cycle and potentially can acquire into the next breath if the breathing cycle shortens. As with respiratory gating, ghost artifacts are reduced, and edge sharpness is restored. However, respiratory triggering requires a long TR as the TR is limited to the respiratory periodicity (or half the respiratory periodicity if the same section is triggered twice during a single respiratory cycle). Respiratory triggering therefore is ideally suited to a fast spin-echo technique where the TR values range from 2000 to 4000 ms, as the typical respiratory cycle in healthy individuals is 4 [9]. Because of the time penalty, respiratory triggering was not used in conjunction with the CSE or STIR sequences, which instead were combined with respiratory compensation (ordered phase encoding). A limitation of this study is that an FSE sequence with and without respiratory triggering were not both included. Our previous work in optimizing the FSE sequence suggested that the RT device was a key factor in determining image quality. We therefore did not include an FSE sequence without respiratory triggering and hence we are unable to prove the specific contribution of the respiratory triggering device to the FSE images obtained in this study.

Artifact caused by high signal subcutaneous fat, which is spread across the phase-encoding direction with respiration, is particularly troublesome with FSE due to the increased signal obtained from fat in this sequence. In a recent study of FSE in the abdomen, FSE sequences combined with fat saturation were preferred over non–fat-suppressed FSE for lesion detection and for detection of areas of signal abnormality [8]. Accordingly, we used fat saturation with our FSE sequence. Fat saturation, however, may be inconsistent due to magnetic field inhomogenity and may have contributed to artifact on some of our FSE images. A further consequence of our use of fat suppression with the FSE sequence is that fat-suppressed sequences (R. trig. FSE and STIR) are compared with a non–fat-suppressed sequence, CSE. As a result certain lesions (e.g., differing fat content or T2 relaxation time) might be perferentially seen on FSE as opposed to CSE sequences.

Our study demonstrated equivalent values for organ contrast and lesion contrast with R. trig. FSE and CSE by using signal-to-noise data. Previous reports on abdominal FSE have shown higher [5], lower [4], and equivalent [19] ratios of signal-to-noise compared with CSE. Each study, however, varies in the FSE imaging parameters used. In the study by Outwater et al. [4], the low signal-to-noise ratio seen on FSE may relate to the use of an echo train of 16, which may be associated with more image blurring than an echo train of 8. Also in that study, neither respiratory compensation nor flow compensation was available for the FSE sequence, leading to an increase in the noise value related to motion artifacts. The clinical significance of these differences in signal-to-noise data is as yet unclear. Our results are based on a small sample size and will require validation in a larger series.

The R. trig. FSE sequences detected both a greater total number of lesions and a higher mean number of lesions than the other sequences, although the results did not reach significance for both readers. However, as we required identification of all lesions on at least two sequences before inclusion, our methodology may have underestimated the sensitivity of any one individual sequence. Of more importance, perhaps clinically, the R. trig. FSE sequence appears to find fewer patients with no detectable abnormality, although true sensitivity cannot be determined without a gold standard technique. In view of the known inability of both MR and CT techniques to detect all hepatic metastatic lesions [26, 27], this potential increase in sensitivity may be important. A criticism of this paper is the inability to provide biopsy proof of the nature of every focal hepatic lesion detected, as it is not practical to biopsy all lesions. However, for the majority of patients with known malignancy who undergo hepatic MR imaging and who are surgical candidates, the essential task is to identify the maximum number of potentially malignant lesions. These lesions may then be evaluated by other imaging techniques or by exploratory surgery. In this regard the R. trig. FSE sequence performs as well as our conventional spin-echo sequences.

In this study, no difference was seen between the sequences in terms of the minimum size of lesions detected. It has been suggested that, due to a broad point-spread function with R. trig. FSE imaging, signal loss may occur with small objects that may then be overlooked [28]. Our results did not confirm this observation and are in agreement with Outwater et al. [4], who found no correlation between signal intensity ratio (signal lesion/signal liver) of liver lesions and lesion size.

Both signal intensity ratios and signal difference-to-noise ratios with lesion morphology have been advocated as a means of differentiating benign from malignant hepatic lesions [4, 29, 30]. The small number of definitely benign lesions (three) found in this study does not allow us to test the value of R. trig. FSE–derived signal measurements. The importance of lesion morphology similarly could not be assessed. The R. trig. FSE images did show the internal structure and the mar-

gins of hepatic lesions to best advantage. The clinical usefulness of this information will require further evaluation.

In summary, R. trig. FSE sequence combined with flow compensation produces hepatic images of comparable diagnostic quality to conventional T2-weighted spin echo images. The R. trig. FSE sequence has a high degree of patient acceptability and is acquired in 5–7 min, which is approximately half the time of the CSE sequence. Although our study population is small, we believe further study to determine the true sensitivity and specificity of this technique is warranted.

References

1. Foley WD, Kneeland JB, Cates JD, et al. Contrast optimization for the detection of focal hepatic lesions by MR imaging at 1.5 T. *AJR* 1987;149:1155–1160
2. Ehman RL, McNamara MT, Brasch RC, et al. Influence of physiologic motion on the appearance of tissue in MR imaging. *Radiology* 1986;159:777–782
3. Mitchell DG, Vinitski S, Burk DL, et al. Motion artifact reduction in MR imaging of the abdomen: gradient moment nulling versus respiratory-sorted phase encoding. *Radiology* 1988;169:155–160
4. Outwater EK, Mitchell DG, Vinitski S. Abdominal MR imaging: evaluation of a fast spin-echo sequence. *Radiology* 1994;190: 425–429
5. Low RN, Francis IR, Sigeti JS, et al. Abdominal MR imaging: comparison of T2-weighted fast and conventional spin-echo, and contrast-enhanced fast multiplanar spoiled gradient-recalled imaging. *Radiology* 1993;186:803–811
6. Catasca JV, Mirowitz SA. T2-weighted MR imaging of the abdomen: fast spin-echo vs conventional spin-echo sequences. *AJR* 1994;162:61–67
7. Nghiem HV, Herfkens RJ, Francis IR, et al. The pelvis: T2-weighted fast spin echo MR imaging. *Radiology* 1992;185:213–217
8. Schwartz LH, Seltzer SE, Tempany CMC, et al. Prospective comparison of T2-weighted fast spin-echo, with and without fat suppression, and conventional spin-echo pulse sequences in the upper abdomen. *Radiology* 1993;189:411–416
9. van Vaals JJ, van Yperen GH. Optimization of T2-weighted turbo spin echo in breath-holding imaging [Abstract]. *JMRI* 1992; 2(P):104
10. Rofsky NM, Weinreb JC, Haddad JL. T2-weighted breath-hold fat-suppressed RARE (turbo SE) imaging of the liver with 15 mT/m gradients at 1.0T [Abstract]. *JMRI* 1993;3(P):68
11. Lewis CE, Prato FS, Drost DJ, et al. Comparison of respiratory triggering and gating techniques for the removal of respiratory artifacts in MR imaging. *Radiology* 1986;160:803–810
12. Reinig JW, Dwyer AJ, Miller DL, et al. Liver metastases: detection with MR imaging at 0.5 and 1.5 T. *Radiology* 1989;170:149–153
13. Steinberg HV, Alarcon JJ, Bernardino ME. Focal hepatic lesions: comparative MR imaging at 0.5 and 1.5 T. *Radiology* 1990; 174:153–156
14. Paulson EK, Baker ME, Paine SS, et al. Detection of focal hepatic masses. STIR MR Vs. CT during arterial portography. *JCAT* 1994;18 (4):581–587
15. Constable RT, Anderson AW, Zhong J, et al. Factors influencing contrast in fast spin-echo MR imaging. *Mag Res Imag* 1991; 10:497–511
16. Spritzer CE, Keogan MK, MacFall J, Dahlke J. Optimizing FSE acquisition for hepatic imaging [Abstract]. *JMRI* 1994;4(P):43
17. Stark DD, Hendrick RE, Hahn PF, et al. Motion artifact reduction with fast spin-echo imaging. *Radiology* 1987;164:183–191
18. Kaufman L, Kramer DM, Crooks LE, et al. Measuring signal-to-noise ratios in MR imaging. *Radiology* 1989;173:265–267
19. Semelka RC, Simm FC, Recht M, et al. T1-weighted sequences for MR imaging of the liver: comparison of three techniques for single-breath, whole-volume acquisition at 1.0 and 1.5T. *Radiology* 1991;180:629–635
20. Hennig J, Nauerth A, Friedburg H. RARE imaging: a fast imaging method for clinical MR. *Mag Res Med* 1986;3:823–833
21. Constable RT, Smith RC, Gore JC. Signal-to-noise and contrast in fast spin echo (FSE) and inversion recovery FSE imaging. *J Comput Assist Tomogr* 1992;16:41–47
22. Mulkern RV, Wong STS, Winalski C, et al. Contrast manipulation and artifact assessment of 2D and 3D rare sequences. *Mag Res Imag* 1990;8:557–566
23. Winkler ML, Thoeni RF, Luh N, et al. Hepatic neoplasia: breath-hold MR imaging. *Radiology* 1989;170:801–806
24. Runge VM, Clanton JA, Partain CL, et al. Respiratory gating in magnetic resonance imaging at 0.5 Tesla. *Radiology* 1984;151: 521–523
25. Ehman RL, McNamara MT, Pallack M, et al. Magnetic resonance imaging with respiratory gating: techniques and advantages. *AJR* 1984;143:1175–1182
26. Wernecke K, Rummeny E, Bongartz G, et al. Detection of hepatic masses in patients with carcinoma: comparative sensitivities of sonography, CT, and MR imaging. *AJR* 1991;157:731–739
27. Nelson RC, Chezmar JL, Sugarbaker PH, et al. Hepatic tumors: comparison of CT during arterial portography, delayed CT, and MR imaging for preoperative evaluation. *Radiology* 1989;172: 27–34
28. Constable RT, Gore JC. The loss of small objects in variable TE imaging: implications for FSE, RARE, and EPI. *Mag Res Med* 1992;28:9–24
29. Egglin TK, Rummeny E, Stark DD, et al. Hepatic tumors: quantitative tissue characterization with MR imaging. *Radiology* 1990; 176:107–110
30. Itoh K, Saini S, Hahn PF, et al. Differentiation between small hepatic hemangiomas and metastases on MR images: importance of size-specific quantitative criteria. *AJR* 1990;155:61–66